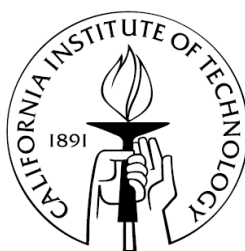


AMBIENT AND LABORATORY STUDIES OF
AEROSOL SIZE DISTRIBUTIONS AND HYGROSCOPICITY

Thesis by
Varuntida Varutbangkul

In Partial Fulfillment of the Requirements
for the Degree of
Doctor of Philosophy



California Institute of Technology

Pasadena, California

2006

(Defended May 22, 2006)

© 2006

Varuntida Varutbangkul

All Rights Reserved

Acknowledgements

First and foremost, I express my sincere gratitude to my advisors, Professor John Seinfeld and Professor Richard Flagan, for their insights, patience, and support for my work throughout the years. Despite their busy schedules, they have always made time to meet and discuss any concerns I had. I especially appreciate their trust, which allowed me to work independently, to gain a wide range of experiences, both in the lab and in the field, and to present my work at conferences. Their scientific knowledge and insight are invaluable, and I feel extremely fortunate to have been under their guidance. I also thank my thesis committee members: Professor Michael Hoffmann and Professor Hafliði Jonsson for their valuable time.

Since a considerable amount of work I did here involved field measurements, I thank the CIRPAS crew for making my time there productive as well as enjoyable. Thanks to Haf for making sure the entire payload runs like a well-oiled machine, Roy and Mike for piloting the Twin Otter to achieve the science objectives (even if that entailed flying into an intimidating updraft), Nava for making sure my LabVIEW program did not cause the instrument to self-destruct, Gintas for operating the DACAD on the plane, and Reggie, Dennis, and Paul for keeping the Otter healthy week after week.

I have been fortunate to be part of a dynamic, friendly, and fun research group. I thank all the past and present members of the group that I have interacted with, especially the “Roofians” and “Fieldians” whom I have had the pleasure to work with closely: Tracey, Sally, Melita, Jesse, Jay, Bill, Armin, Shane, Jason, Harmony, Song, Jose, and Dara. Together we survived multiple long trips on the U-Hauls, lifted a million cumulative pounds of instruments into the plane, tracked down holes in the smog

chamber, and worked through the stressful periods. Working with all of you has been a great experience. Tracey Rissman deserves special thanks for sharing her insights and carrying on lengthy discussions with me to unravel the experimental mysteries, and of course for being a great friend and tolerating my night-owl schedule in the apartment. Without her and Adam Olsen, the last few months would have been much more stressful.

I am grateful to Mike Vondrus, who expertly machined various parts of my experimental setup and David Cocker who answered my daily questions about the roof instruments in my first year in lab. I also appreciate the help of Fred Brechtel who helped to provide insights to the HTDMA issues and the data. Also, none of this work would have been possible without the administrative help of Ann Hilgenfeldt and Yvette Grant for placing endless orders for parts and repairs. Thank you!

I am glad to have met many friends outside the lab who have made my time at Caltech enjoyable: Mike, Nikoo, Adam, Anita, Philip, Marco, Karen, Paul, Jon, and Soojin. Whether we were working on problem sets, running 26 miles, or satisfying our hunger and thirst, I truly appreciate your companionship. I also express heartfelt thanks to Desiree LaVertu, Don Caldwell, and Delores Bing, who, by virtue of having nothing to do with science, gave me an outlet for stress with their gift of music. Your kindness has been a blessing to me, and I would not have survived graduate school otherwise.

Finally, I thank my parents for their love and sacrifice, which allowed me to pursue my education far from home and to strive to be a well-rounded and independent person. I am infinitely grateful to them for teaching me never to give up and instilling in me the love of learning since a young age. Without their continuing support and encouragement, I would not be where I am today.

Abstract

The optical properties, health effects, atmospheric lifetime, and climate impact of ambient aerosols are influenced directly by their size distribution, chemical composition, and phase. The aerosol hygroscopicity, which is also a function of composition, governs the size and phase changes of these particles when subjected to varying ambient relative humidities (RH). This thesis presents results from a wide variety of studies involving laboratory and ambient measurements of aerosol size distributions and water uptake properties in the subsaturated regime. Time evolutions of particle size and hygroscopic growth were investigated for various secondary organic aerosol (SOA) systems generated in a smog chamber from ozonolysis of cycloalkenes and photooxidation of biogenic terpenes. SOA yields were measured at various initial parent hydrocarbon concentrations and correlated with the structure of the parent compound. The amount of water uptake of the aerosol at a reference RH was found to inversely correlate with the SOA yield. The hygroscopicity of many atmospherically relevant pure organic species was also studied using an unconventional particle generation scheme employing a nonaqueous solution. Experimental results were compared with predictions from an equilibrium thermodynamic model. In these works, organic aerosols are shown to exhibit complex hygroscopic growth, dependent on the particle chemistry, phase, and surrounding RH. Implications of the experimental techniques used on the observation of particle growth, deliquescence, and efflorescence are discussed. A number of other studies incorporating aircraft-based measurements of aerosol size distributions and hygroscopicity with other ambient measurements into various cloud microphysics models are also presented.

Table of Contents

Acknowledgements	iii
Abstract	v
List of Tables	xi
List of Figures	xiii
1 Introduction	1
2 Secondary Organic Aerosol Formation from the Ozonolysis of Cycloalkenes and Related Compounds	5
2.1 Abstract	6
2.2 Introduction	7
2.3 Experimental description	10
2.4 Results and discussion	14
2.4.1 SOA yields	14
2.4.2 Yield and carbon number	15
2.4.3 Yield and the presence of a methyl group	16
2.4.4 Yield and the presence of an exocyclic double bond	17
2.4.5 Yield curve for terpinolene	17
2.4.6 Yield and compound structure: Multivariate relationships	18
2.4.7 Yield and structure: Discussion	19
2.5 Acknowledgements	21
2.6 References	22
Tables and figures.....	26

3	Hygroscopicity of Secondary Organic Aerosols Formed by Oxidation of Cycloalkenes, Monoterpenes, Sesquiterpenes, and Related Compounds	38
3.1	Abstract	39
3.2	Introduction	41
3.3	Experimental methods	46
3.3.1	SOA generation in the smog chamber	46
3.3.1.1	Cycloalkene ozonolysis	46
3.3.1.2	Terpene photooxidation	48
3.3.2	Analytical instrumentation	49
3.3.2.1	Chamber instrumentation	49
3.3.2.2	Hygroscopicity tandem differential mobility analyzer (HTDMA)	50
3.4	Results and Discussion	54
3.4.1	Cycloalkene ozonolysis	54
3.4.1.1	Seeded experiments: SOA formation on inorganic substrate ...	54
3.4.1.2	Nucleation experiments: Pure SOA	56
3.4.2	Terpene photooxidation	58
3.4.2.1	Sesquiterpenes: Nucleated SOA	58
3.4.2.2	Monoterpenes and oxygenated terpenes: SOA on inorganic seed	62
3.4.3	Mass transfer considerations	70
3.4.4	Comparison of growth factors from various systems	71
3.5	Conclusions	72

3.6	Acknowledgements	74
3.7	References	75
	Tables and figures.....	87
4	Hygroscopicity of Atmospherically Relevant Organic Aerosols.....	109
4.1	Abstract	110
4.2	Introduction	112
4.3	Experimental methods	114
4.3.1	Aerosol generation	114
4.3.2	Hygroscopicity tandem differential mobility analyzer (HTDMA)	116
4.3.3	ADDEM thermodynamic model	120
4.4	Results and discussion	122
4.4.1	Dicarboxylic acids	122
4.4.2	Amino acids	135
4.4.3	Other multifunctional acids	139
4.4.4	Fatty acids and steroid	142
4.4.5	Comparison of growth factors of different organic species	142
4.5	Conclusions	143
4.6	Acknowledgements	146
4.7	References	147
	Tables and figures.....	157
5	Conclusions and Future Studies	177

Appendix A: New Particle Formation from Photooxidation of Diiodomethane (CH ₂ I ₂)	184
Appendix B: Toward Aerosol/Cloud Condensation Nuclei (CCN) Closure During CRYSTAL-FACE	211
Appendix C: Effect of Relative Humidity on the Detection of Sulfur Dioxide and Sulfuric Acid Using a Chemical Ionization Mass Spectrometer	230
Appendix D: Evidence for the Predominance of Mid-Tropospheric Aerosols as Subtropical Anvil Cloud Nuclei	245
Appendix E: Secondary Organic Aerosol Formation from Cyclohexene Ozonolysis: Effect of OH Scavenger and the Role of Radical Chemistry	251
Appendix F: Aerosol-Cloud Drop Concentration Closure in Warm Cumulus	260
Appendix G: Low-Molecular-Weight and Oligomeric Components in Secondary Organic Aerosol from the Ozonolysis of Cycloalkenes and Alpha-pinene	273
Appendix H: Particle Phase Acidity and Oligomer Formation in Secondary Organic Aerosol	292
Appendix I: Measurements of Secondary Organic Aerosol from Oxidation of Cycloalkenes, Terpenes, and m-xylene Using an Aerodyne Aerosol Mass Spectrometer	301
Appendix J: Anvil Glaciation in a Deep Cumulus Updraught over Florida Simulated with the Explicit Microphysics Model. I: Impact of Various Nucleation Processes	317

Appendix K: Chamber Studies of Secondary Organic Aerosol Growth by Reactive Uptake of Simple Carbonyl Compounds	346
Appendix L: Contribution of First- Versus Second-Generation Products to Secondary Organic Aerosols Formed in the Oxidation of Biogenic Hydrocarbons	357
Appendix M: Gas-Phase Products and Secondary Aerosol Yields from the Ozonolysis of Ten Different Terpenes	373
Appendix N: Airborne Aerosol Flux Measurements with Eddy Correlation above the Ocean in a Coastal Environment	392

List of Tables

Table 2.1	Structures of parent hydrocarbons investigated in this study	26
Table 2.2	Initial conditions and data for alkene ozonolysis experiments	27
Table 2.3	Aerosol yield parameters for the ozonolysis of cycloalkenes and related compounds	29
Table 2.4	Matrix of correlation coefficients	30
Table 3.1	Previous studies involving hygroscopicity or CCN activity of secondary organic aerosols.....	87
Table 3.2	Hydrocarbon precursors studied	88
Table 3.3	Summary of nucleation experiments performed and fitting results of the final hygroscopic growth curve	90
Table 3.4	Effective particle density and SOA density for monoterpene and oxygenated terpene precursors used in seeded experiments, in which AMS measurements were available	91
Table 3.5	Summary of experiments with $(\text{NH}_4)_2\text{SO}_4$ seed, fitting results of the hygroscopic growth curve, and pure SOA growth factors (GF_{org}) calculated from measured organic fractions at different TDMA-classified sizes	92

Table 4.1	Organic species studied	157
Table 4.2	Experimental summary, curve fitting results of the final hygroscopic growth curve, and GF at 85% RH calculated from the fit curve for each organic compound studied	160
Table 4.3	Growth factor predictions by the ADDEM model given various input combinations of UNIFAC parameters, surface tension models, and dry and liquid density parameters for oxalic acid (courtesy of D. O. Topping and G. B. McFiggans)	161

List of Figures

Figure 2.1	Structure of parent hydrocarbons investigated in this study	31
Figure 2.2	SOA yield data and curves fitted by Eq. (2.1) as a function of ΔM_o for the cycloalkenes	32
Figure 2.3	SOA yield data and curves fitted by Eq. (2.1) as a function of ΔM_o for (a) cyclopentene and 1-methylcyclopentene, (b) cyclohexene and 1-methylcyclohexene, and (c) cycloheptene and 1-methylcycloheptene	33
Figure 2.4	Yield SOA yield data and curves fitted by Eq. (2.1) as a function of ΔM_o for (a) cyclohexene and 1-methylcyclopentene, (b) cycloheptene and 1-methylcyclohexene and, (c) cyclooctene and 1-methylcycloheptene	34
Figure 2.5	SOA yield data and curves fitted by Eq. (2.1) as a function of ΔM_o for cyclohexene, 1-methylcyclohexene and 3-methylcyclohexene	35
Figure 2.6	SOA yield data and curves fitted by Eq. (2.1) as a function of ΔM_o for terpinolene relative to cyclohexene, 1-methylcyclohexene and methylenecyclohexane	36
Figure 2.7	Initial reactions of ozone with the main cycloalkene structures to form Criegee intermediates	37

Figure 3.1	Schematic of the HTDMA system used	93
Figure 3.2	Image plots of raw HTDMA data and the variations in RH in a typical operating scheme for (a) cycloalkene ozonolysis experiments (dry) and (b) terpene photooxidation experiments (humid)	94
Figure 3.3	Aerosol hygroscopic growth factor decreases as the precursor cycloalkene is consumed and the gas-to-particle partitioning of organic products occurs onto $(\text{NH}_4)_2\text{SO}_4$ seed	95
Figure 3.4	Bimodal size distribution of grown droplets at classified diameter of 180 nm, observed during early times in experiments	96
Figure 3.5	Time series of the particle number concentration (as measured by CPC) and mode diameter of the chamber aerosol and the TDMA growth factor in two cycloalkene ozonolysis nucleation experiments	97
Figure 3.6	Hygroscopic growth factor as a function of RH for nucleated SOA formed by ozonolysis of 170 ppb of cycloheptene	98
Figure 3.7	Fitted curves of hygroscopic growth factors as a function of RH for nucleated SOA formed by ozonolysis of various cycloalkenes. Fitting parameters used to generate the curves are given in Table 3.3	99
Figure 3.8	The percent volumetric water content (at chamber RH) of nucleated sesquiterpene photooxidation SOA decreases with time during the experiment, suggesting that the SOA is becoming less hygroscopic	100
Figure 3.9	Different classified diameters of pure β -caryophyllene photooxidation SOA exhibit similar hygroscopic growth factors, suggesting that the aerosol composition is independent of particle size.	101

Figure 3.10	Hygroscopic growth curves for nucleated SOA formed by sesquiterpene photooxidation	102
Figure 3.11	The percent volumetric water content (at chamber RH) at a particular particle size of SOA formed by photooxidation of monoterpene and oxygenated terpene decreases with time early in experiment due to the deposition of less-hygroscopic organic species onto the seed	103
Figure 3.12	Hygroscopic growth curve for linalool photooxidation SOA, measured at 180 nm and 300 nm. The differing hygroscopicity reflects the different organic fractions at each size	104
Figure 3.13	Raw hygroscopic growth factors of SOA from monoterpene and oxygenated terpene photooxidation (with $(\text{NH}_4)_2\text{SO}_4$ seed)	105
Figure 3.14	Size-dependent organic mass fraction vs. particle vacuum aerodynamic diameter, as measured by the AMS at various times during linalool photooxidation experiment	106
Figure 3.15	Hygroscopic growth curves of (a) Δ^3 -carene, (b) linalool, and (c) limonene photooxidation SOA, with and without accounting for the effect of water uptake by inorganic seed	107
Figure 3.16	SOA growth factor versus (a) the molecular weight and (b) the SOA yield of the precursor	108

Figure 4.1	Schematic of the HTDMA system used	162
Figure 4.2	Hygroscopic growth curves for succinic acid and adipic acid	163
Figure 4.3	Hygroscopic growth curve for oxalic acid	164
Figure 4.4	Aerosol size distributions detected by the scanning DMA of dry 400-nm classified glutaric acid particles	165
Figure 4.5	Hygroscopic growth curve for glutaric acid	166
Figure 4.6	Hygroscopic growth curves for malonic acid aerosol generated from (a) a methanol solution and (b) an aqueous solution	167
Figure 4.7	Hygroscopic growth curve of phthalic acid	168
Figure 4.8	Hygroscopic growth curve for DL-leucine	169
Figure 4.9	Hygroscopic growth curve for DL-glutamic acid monohydrate	170
Figure 4.10	Hygroscopic growth curve for DL-malic acid	171
Figure 4.11	Hygroscopic growth curve for 2-hydroxycaproic acid	172
Figure 4.12	Hygroscopic growth curve for cis-pinonic acid	173
Figure 4.13	Hygroscopic growth curve for sinapic acid	174
Figure 4.14	Hygroscopic growth curves of (a) myristic acid, (b) palmitic acid, (c) stearic acid, and (d) cholesterol	175
Figure 4.15	Hygroscopic growth factors at 85% RH calculated from the curve fit to the data of various organic species plotted against (a) the pK_a and (b) the water solubility of the organic compound	176

Chapter 1
Introduction

Introduction

Aerosols are ubiquitous in the atmosphere and are emitted or formed by both natural processes and anthropogenic activities. These particles affect human health, regional visibility, formation of clouds and precipitation, as well as the earth's overall energy balance, which can have far-reaching implications such as climate change. Understanding the ways in which aerosols behave, evolve, and exert these effects requires the knowledge of their formation and removal mechanism, transport processes, as well as their physical and chemical characteristics. The particle properties relevant in determining the aforementioned effects include the number concentration, size distribution, chemical composition, reactivity with other species, and response to environmental states. The hygroscopicity, i.e., the tendency for a particle to take up water, also influences the particle size distribution, phase, and degree of activity as cloud condensation nuclei, which can all in turn affect the atmospheric lifetime of the particle. Recent studies have shown that atmospheric aerosols are a complex mixture of inorganic species, such as salts and elementary carbon, and the organic fraction that can comprise hundreds of species, representing a wide variety of compound classes and origins. Unraveling the pathways responsible for forming these particles and understanding the physical and chemical changes these particles undergo in the ambient atmosphere are still very much a work in progress.

This thesis presents results from a wide range of laboratory and field experiments aimed at understanding the formation mechanism and physical and chemical characterization of submicron aerosol. Specifically, the focus has been placed on the measurements of particle size distribution and hygroscopic growth. In Chapter 2,

formation of secondary organic aerosols (SOA) in a laboratory smog chamber is described and the yields from a family of cycloalkenes are reported. Through a large number of ozonolysis experiments, the yield curves illustrating the relationship between the SOA yield and the absolute amount of organic mass formed can be generated. The relative aerosol-forming potential of different precursors is discussed on the basis of several aspects of the parent hydrocarbon structure.

In Chapter 3, hygroscopic behavior of the SOA formed in the smog chamber is presented. The parent compounds used to generate the SOA range from model compounds such as cycloalkenes of various carbon numbers and substitutions to atmospherically relevant biogenic terpenoid compounds. Using the hygroscopicity tandem differential mobility analyzer (HTDMA), measurements of the water uptake of these SOA as a function of time, particle size, and relative humidity are performed. The results are presented in the form of hygroscopic growth curves and time evolution of particle water content. In mixed organic-inorganic particles, hygroscopicity of the organic portion is calculated using a simple volume-weighting model and complementary measurement of organic fraction using the Aerodyne aerosol mass spectrometer.

Chapter 4 summarizes a set of laboratory measurements on the water uptake properties of a variety of pure organic species, including straight-chain and aromatic dicarboxylic acids, multifunctional acids, amino acids, fatty acids, and a steroid. The HTDMA-derived hygroscopic growth curves are compared with predictions from a thermodynamic model and with previous studies using different particle generation schemes and measurement techniques. Chapter 5 summarizes the findings discussed in the previous three chapters and provides suggestions for future studies.

The appendices at the end of this thesis contain results from various works in the laboratory and field campaigns. Appendices A, E, G–I, and K–M present findings from a variety of smog chamber studies on secondary aerosol formation, encompassing systems such as diiodomethane ozonolysis in the presence of UV light, cycloalkene ozonolysis, m-xylene photooxidation, terpene ozonolysis and photooxidation, and reactive uptake of carbonyl compounds onto preexisting particles. Parameters in nucleation phenomenon, aerosol yield, potential oxidation mechanism, and chemical composition of both the aerosol- and gas-phase oxidation products measured in real time and in bulk form are presented.

Appendix C describes findings on the detection of sulfur dioxide and sulfuric acid at high humidities using the chemical ionization mass spectrometer. A new ionization scheme and the effect of RH on the detection are discussed. Appendices B, D, F, J and N present a variety of observational and modeling studies that integrate measurements aboard the CIRPAS Twin Otter and other aircraft to investigate particle activation and the microphysics of cloud formation. Aerosol size distributions measured with the Caltech twin differential mobility analyzers (also known as Dual Automated Classified Aerosol Detector or DACAD) were used in these studies along with measurements of fine aerosol number concentrations, cloud condensational nuclei concentrations, submicron aerosol chemical composition, updraft velocities, and cloud droplet number and droplet size distributions.